JACS
JOURNAL OF THE AMERICAN CHEMICAL SOCIETY
Article
pubs.acs.org/JACS

Site-Specific Protonation Kinetics of Acidic Side Chains in Proteins Determined by pH-Dependent Carboxyl ^{13}C NMR Relaxation

Johan Wallerstein,[†] Ulrich Weininger,[†] M. Ashhar I. Khan,[†,§] Sara Linse,[‡] and Mikael Akke*[,†]

[†]Department of Biophysical Chemistry and [‡]Department of Biochemistry and Structural Biology, Center for Molecular Protein Science, Lund University, P.O. Box 124, SE-221 00 Lund, Sweden

[§]Department of Chemistry, Indian Institute of Technology Delhi, Hauz Khas, New Delhi 110 016 India

Supporting Information

ABSTRACT: Proton-transfer dynamics plays a critical role in many biochemical processes, such as proton pumping across membranes and enzyme catalysis. The large majority of enzymes utilize acid−base catalysis and proton-transfer mechanisms, where the rates of proton transfer can be rate limiting for the overall reaction. However, measurement of proton-exchange kinetics for individual side-chain carboxyl groups in proteins has been achieved in only a handful of cases, which typically have involved comparative analysis of mutant proteins in the context of reaction network modeling. Here we describe an approach to determine site-specific protonation and deprotonation rate constants (k_{on} and k_{off}, respectively) of carboxyl side chains, based on ^{13}C NMR relaxation measurements as a function of pH. We validated the method using an extensively studied model system, the B1 domain of protein G, for which we measured rate constants k_{off} in the range $(0.1-3) \times 10^6$ s^{-1} and k_{on} in the range $(0.6-300) \times 10^9$ M^{-1} s^{-1}, which correspond to acid−base equilibrium dissociation constants (K_a) in excellent agreement with previous results determined by chemical shift titrations. Our results further reveal a linear free-energy relationship between log k_{on} and pK_a, which provides information on the free-energy landscape of the protonation reaction, showing that the variability among residues in these parameters arises primarily from the extent of charge stabilization of the deprotonated state by the protein environment. We find that side-chain carboxyls with extreme values of k_{off} or k_{on} are involved in hydrogen bonding, thus providing a mechanistic explanation for the observed stabilization of the protonated or deprotonated state.

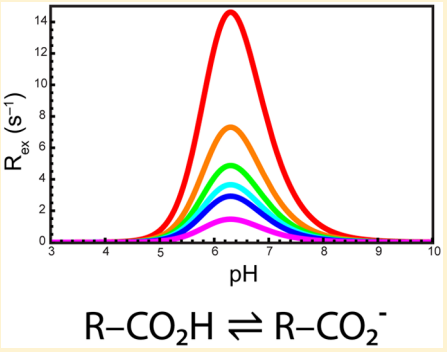

INTRODUCTION

Proteins are dynamic entities whose equilibrium properties are best described in terms of ensembles of interconverting substates. Their properties and functions result in large part from their noncovalent interactions, which dominate biomolecular recognition. Electrostatic forces are particularly important due to their long-range nature. The electrostatic properties of proteins depend on the local arrangement of ionizable side chains, the pH of the surrounding solvent, and the concentration of all charged species in the solution, which govern the equilibrium distribution of charged and noncharged states of individual side chains.[1−5] In addition, interactions with ligands, membranes, proteins, or other biomolecules can also affect the acid−base equilibrium dissociation constant, K_a.[6] The pK_a values of individual titrating side-chain groups of aspartic (D) and glutamic (E) amino-acid residues often exhibit shifts from the canonical values expected for the isolated amino acid in solution, as a result of interactions with other charged sites in the protein or of hydrogen bonding involving the carboxyl group.[7−9] Up-shifted pK_a values are commonly observed for carboxyl groups in enzyme active sites,[7,8,10] where proton-transfer reactions are central to the catalytic mechanisms.[11−14]

In addition to the equilibrium distributions of protonated (noncharged) and nonprotonated (charged) carboxyl groups, the rates of exchange between these states are critically important for a diverse array of biological processes,[15] including proton pumping[16−23] in addition to enzyme catalysis. The very large majority of enzyme-catalyzed reactions involves acid−base catalysis and proton-transfer mechanisms.[13,24] The proton-exchange rates of reacting groups and neighboring residues are of central importance as they determine the average rates of proton transfer and subsequent re-equilibration within the proton-transfer network, during and following the reaction steps, which might be rate limiting for the overall reaction in question.[2,14,15,23,25−27] Thus, quantifying proton exchange in protein side-chains represents a key step forward toward understanding the dynamics of certain classes of biochemical reactions.

The rate of proton exchange also has ramifications for computational approaches for estimating pK_a and for investigating the mechanisms of enzyme catalysis or ligand binding, as follows. Detailed comparisons have shown that pK_a calculations can be improved significantly if conformational sampling is taken into account by performing calculations over multiple molecular dynamics (MD) trajectories.[28] Because

Received: December 28, 2014
Published: February 10, 2015

DOI: 10.1021/ja513205s
J. Am. Chem. Soc. 2015, 137, 3093−3101

conformational fluctuations are expected to depend on the (local) electrostatic field, the binary variation in charge of individual side chains becomes important.[9,29,30] If the mean lifetime of the charged state of each side chain is much shorter than the characteristic time scale of conformational fluctuations, then it might be permissible to approximate the distribution of charged and uncharged side chains across the ensemble by a partial charge in a single structure. However, if the mean lifetime of the charged state is comparable to or longer than the conformational fluctuations, then an ensemble representation is required to capture the full distribution of charge and conformational states, which amounts to a formidable computational challenge when the number of titrating sites is large. This problem further underlines the importance of characterizing both conformational dynamics and protonation kinetics for understanding biomolecular function.

Experimental data on proton-transfer rates are relatively scarce and currently lag behind computational studies.[31] By contrast, there is a long history of using NMR spectroscopy to determine site-specific pK_a values by recording the variation in chemical shifts of titrating residues as a function of pH, which have served as benchmarks for a large number of computational investigations of protein electrostatics.[7,8,10,32−36] Experimental methods for measuring proton-transfer rates include IR spectroscopy[17] and fluorescence correlation spectroscopy,[37,38] which are both limited in site resolution by requiring specific labeling that involves significant efforts to provide system-wide information. NMR relaxation measurements on water have been used to characterize proton transfer between water and carboxylic acids,[39−41] but this method cannot provide site-specific information on proton-transfer rates of protein side chains. Intrinsic proton-exchange rates of hydroxyl groups, the arginine guanidinium group, and the lysine amino group in isolated amino acids have been characterized by ^{1}H NMR line-width measurements.[42] More recently, elegant methods have been devised to study site-specific proton exchange in arginine, lysine, and histidine side chains in proteins, based on scalar relaxation of ^{15}N nuclei, caused by the exchange of protons that are covalently bound directly to the heteronucleus and consequently have a large one-bond coupling constant ($^1J_{NH}$ ≈ −98 to −73 Hz).[43−45] Proton exchange in carboxylic side chains cannot be studied by the same approach, because in this case the exchanging proton is attached to oxygen, the only NMR-active isotope of which is ^{17}O, whose magnetic quadrupole moment totally dominates its relaxation properties. Moreover, scalar relaxation of the neighboring ^{13}C nuclei is inefficient due to the small two- or three-bond coupling constants ($^2J_{CH}$ ≈ 5−7 Hz; $^3J_{CH}$ ≈ 4−7 Hz).[46]

Here we extend the repertoire of NMR-based approaches for measuring site-specific proton-exchange rates to encompass also aspartic and glutamic side chains. Theoretical considerations predict that the exchange kinetics of acidic groups in proteins should be very fast, on the order of 10^6 or faster.[11] Thus, we expect that proton-transfer rates are too high, in general, to be measurable by canonical relaxation dispersion experiments, which monitor the effective transverse relaxation rates as a function of refocusing-field frequency using either Carr−Purcell−Meiboom−Gill pulse sequence (CPMG) or rotating-frame spin-lock ($R_{1\rho}$) methods.[47−49] Nevertheless, we demonstrate that the on- and off-rates of proton exchange can be determined from the pH-dependence of the carboxyl ^{13}C transverse relaxation rates, even though the effective relaxation rates do not show any variation with respect to changes in the refocusing frequency at a given pH. The method is advantageously combined with conventional pK_a determination, performed by monitoring the chemical shift as a function of pH, which also provides validation of the results by comparison of pK_a values determined by the two approaches.

We demonstrate the method by measuring protonation kinetics (on- and off-rates) for a suitable model system, namely a variant of the B1 domain of protein G from *Streptococcus sp.* (PGB1, Figure 1), which has been characterized extensively in terms of its electrostatic properties, residue-specific pK_a values, and pH titration behavior.[33,52−57] We find that k_{off} varies in the range (0.1−3) × 10^6 s^{-1} at 25 °C, while k_{on} is approximately 3−5 orders of magnitude greater, with values in the range (0.6−300) × 10^9 M^{-1} s^{-1}. Interestingly, log k_{on} shows a linear free-energy relationship with pK_a, while the residue-to-residue variation in log k_{off} appears more scattered. This result offers insights into the free-energy landscape of the protonation reaction, demonstrating that the extent of charge stabilization dominates the variability in k_{on} and K_a among residues. Furthermore, we find that the carboxyls with the lowest on-rates and lowest pK_a values are hydrogen bonded in the crystal structure, thus providing a mechanistic explanation for the observed effects.

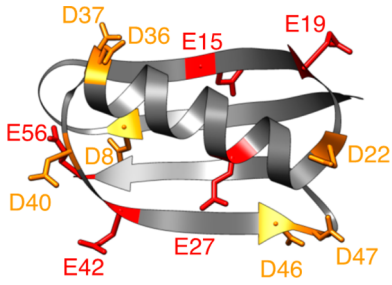

Figure 1. Structure of PGB1-QDD with aspartic (D) and glutamic (E) side chains highlighted in yellow and red, respectively. The model is based on 1pgb.pdb[50] with the following three substitutions: T2Q, N8D, and N37D. The model was prepared using UCSF Chimera.[51]

RESULTS AND DISCUSSION

To determine the proton-exchange kinetics, we measured site-specific transverse relaxation rates (R_2) for ^{13}C side-chain carboxyl or carbonyl spins as a function of pH across the entire transition between the protonated and deprotonated states. In total, we acquired ^{13}C relaxation data at 21 pH values, ranging from 1.9 to 8.5, and two temperatures, 15 and 25 °C. We carried out residue-specific resonance assignments of the $^1H^{\beta/\gamma}$−^{13}CO correlation spectra, based on the reported chemical shifts.[33] In general, the chemical shift dispersion is greater at higher pH, where the carboxyl groups are charged. The $^1H^{\beta/\gamma}$−^{13}CO correlation spectra acquired at different pH values are shown in Figure S1 (Supporting Information).

We redetermined the residue-specific pK_a values from the chemical shift versus pH isotherms (Figure S2) and found them to agree closely with those reported previously (RMSD = 0.16; Figure S3).[53] However, for side chains that have pK_a < 3 (D22 and D47), the present pK_a values tend to differ somewhat from those determined previously, with ΔpK_a = 0.1−0.35 (Figure S3). We tentatively attribute this apparent discrepancy to the lower precision of pK_a estimates in the regime below 3 (Table S1), which arises as a consequence of increased spectral overlap and limited protein stability at low pH.

DOI: 10.1021/ja513205s
J. Am. Chem. Soc. 2015, 137, 3093−3101

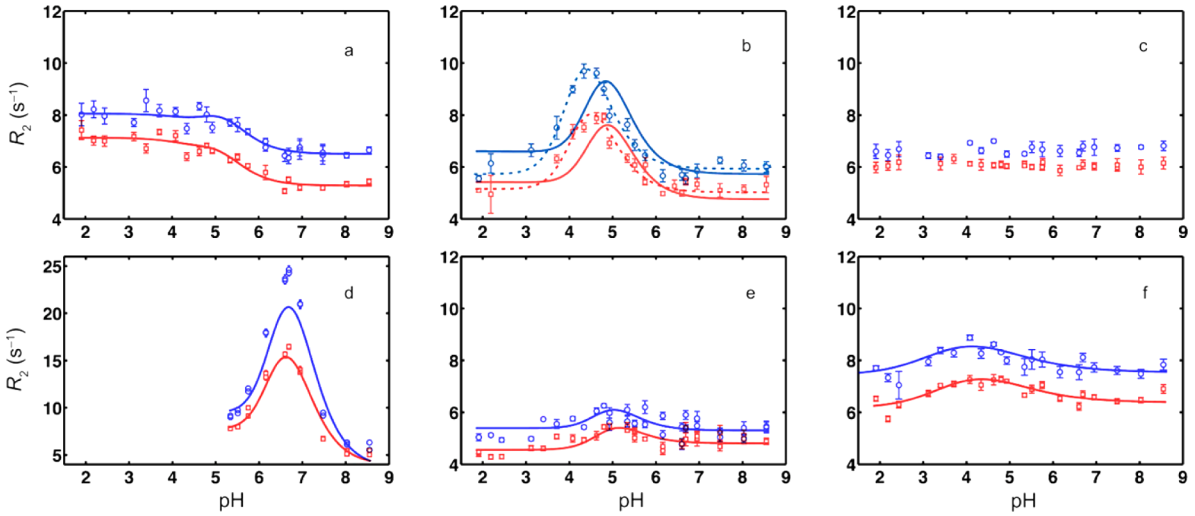

Figure 2. Transverse relaxation rates (R_2) plotted as a function of pH. Results are shown for 6 of the 15 side-chain carboxyl or amide groups in PGB1-QDD: (a) D8, (b) E15, (c) Q32, (d) D37, (e) E42, and (f) E56. The blue and red curves represent fits of eq 7 to the data obtained at temperatures of 15 °C (blue circles) and 25 °C (red squares), respectively. The fitted parameters are k_{off}, $R_{2,A}$, and $R_{2,HA}$, while pK_a and $\Delta\omega$ are fixed at the values obtained from fits of eq 8 to the chemical shift titration curves, and the Hill coefficient is fixed at $n_H = 1$, except for E56 of panel (f) where it is fixed at $n_H = 0.48$ (15 °C) or 0.51 (25 °C). In panel (b), dotted lines represent fits to eq 7 with K_a included as a free parameter. In panel (d), data at pH < 5 have been omitted, because these are affected by an additional conformational exchange process (see the text). Error bars indicate 1 standard deviation.

Electrostatic interactions within networks of titrating residues in proteins render the pK_a values dependent on pH in principle, since the local electric field changes as neighboring residues titrate, leading to significant cooperativity in proton titration behavior.[58,59] We investigated the extent of electrostatic coupling between residues by comparing fits with or without a Hill coefficient (n_H) in eq 8.[32] n_H is an ad hoc parameter generally used to describe nonsymmetric, nonsigmoidal titration curves, e.g., to represent a pH dependence of pK_a. While the inclusion of n_H among the free parameters of the fit is statistically significant for all residues in protein G domain B1 from *Streptococcus sp.* with the mutations T2Q, N8D, and N37D (PGB1-QDD) (Table S1), the results indicate only a modest cooperativity, with n_H ranging from 0.67 to 1.05, except for the C-terminal residue E56, which has $n_H = 0.51$ (at 25 °C) and 0.48 (15 °C). The mean and standard deviation, calculated for all 12 residues (including E56), are $\langle n_H \rangle = 0.80 \pm 0.13$. E56 is the only residue that falls outside of 2 standard deviations from the mean, in agreement with previous observations.[33] The stronger cooperativity exhibited by E56 presumably arises because its side-chain and C-terminal (backbone) carboxyl groups are in close proximity.

Overall, the close agreement between the present and previously determined pK_a values and chemical shift differences validates our current protocol for sample preparation and the resulting data. Next, we went on to extract site-specific proton-exchange rates from ^{13}C R_2 relaxation rates, acquired for the carboxyl side-chain groups of aspartic and glutamic residues.

Site-Specific Proton-Exchange Kinetics. Representative R_2 relaxation rates as a function of pH are shown in Figure 2 (see Figure S4 for an overview of R_2 vs pH dispersion profiles for all residues), which clearly demonstrate the expected dependence of R_2 on pH (cf. Figure 4). In all cases, the data are adequately described by the model represented by eqs 1−7, as described in detail below.

We used the pK_a and $\Delta\omega$ ($= \Delta\delta\gamma B_0$) values determined from the chemical shift titrations as fixed parameters in nonlinear fits to determine $R_{2,A}$, $R_{2,HA}$, and k_{off} from the R_2 vs pH profiles. A simpler two-parameter model, which assumes $R_{2,A} = R_{2,HA}$ is sufficient for many residues but yields k_{off} values very similar to those from the three-parameter model (Table S2). We opted to use the three-parameter model in reporting results for all residues. Fitting the R_2 vs pH profiles with a model that includes pK_a as a fourth free parameter yields pK_a values in good agreement with those determined from the chemical shift data (Table S1). The correlation coefficient r^2 is 0.90 at 25 °C and 0.87 at 15 °C (Figure S5). E15 is the only residue that yields a significantly different pK_a value in these two fits (and a significant improvement in the fit, $p < 0.001$; see Table S2), with values of 4.62 ± 0.01 and 4.20 ± 0.03 resulting from the chemical shift and R_2 data, respectively (Figure 2b); at present we do not know the origin of this discrepancy. In general, pK_a is determined more precisely from the chemical shift titrations than from the relaxation data, with a relative error that is approximately 10 times smaller. $\Delta\omega$ is typically very well determined from chemical shift titrations (see Figure S2). The single exception is D22, which has a significantly down-shifted pK_a value, such that δ_{obs} does not reach a clear plateau at low pH, thus making δ_A (and pK_a) imprecise in this particular case.

In contrast to the case for the chemical shift titrations, there is no significant improvement in the fit of the relaxation data when n_H is included, except for E56, as gauged by comparing the χ^2 values resulting from fits with n_H fixed at 1 or at the value determined from the chemical shift titrations.

The resulting site-specific on- and off-rates vary significantly between residues (Table 1). k_{off} varies by a factor of approximately 30, covering the range between $(0.120 \pm 0.001) \times 10^6$ s^{-1} for D37 and $(3.4 \pm 0.3) \times 10^6$ s^{-1} for D47 at 25 °C. By contrast, k_{on} varies by 3 orders of magnitude, from $(0.13 \pm 0.09) \times 10^9$ M^{-1} s^{-1} for D22 to $(288 \pm 3) \times 10^9$ M^{-1} s^{-1} for D37. Note that k_{on} is expected to reach a maximum value in the diffusion-controlled limit, which is dictated by electrostatic interactions between the reactants and by the effective diffusion constant of the hydronium ion, including

DOI: 10.1021/ja513205s
J. Am. Chem. Soc. 2015, 137, 3093−3101

Table 1. Site-Specific on- And off-Rates for Proton Exchange in Acidic Residues of PGB1-QDD[a]

	k_{off} (10^5 s^{-1})		k_{on} (10^9 s^{-1} M^{-1})	
res	25 °C	15 °C	25 °C	15 °C
D8	22 ± 3	15 ± 2	176 ± 30	139 ± 23
E15	5.9 ± 0.2	5.1 ± 0.2	24.7 ± 0.4	19.5 ± 0.3
E19	18 ± 2	14.1 ± 0.9	10.1 ± 0.6	7.8 ± 0.3
D22	3.0 ± 0.5	2.2 ± 0.3	0.13 ± 0.09	0.09 ± 0.05
E27	6.6 ± 0.2	4.9 ± 0.2	43 ± 1	36.3 ± 0.8
D36	n/a	n/a	n/a	n/a
D37	1.20 ± 0.01	0.83 ± 0.01	288 ± 3	229 ± 3
D40	30 ± 2	29 ± 3	38 ± 1	38.4 ± 0.8
E42	24 ± 2	22 ± 2	158 ± 7	122 ± 9
D46	10 ± 1	8.7 ± 0.8	5.5 ± 0.4	5 ± 2
D47	34 ± 3	32 ± 3	2.2 ± 0.5	2.2 ± 0.2
E56	8.6 ± 0.6	7.8 ± 0.6	4.3 ± 0.2	2.4 ± 0.2

[a]Error estimates are reported as 1 standard deviation.

both molecular diffusion and proton shuttling along hydrogen bonds between water molecules.[11,31] The present results might suggest that proton transfer to D37 has reached the diffusion-controlled limit, because its on-rate is on par with that of D8 and E42, which have significantly lower pK_a values (Table 1; Figure 3a). Furthermore, maximum k_{on} values on the order of 10^{11} M^{-1} s^{-1} are in line with theoretical expectations.[11] The limiting on-rate imposed by diffusion control implies that carboxyls with highly up-shifted pK_a values should have low k_{off} values; D37 is a case in point with its significant relaxation dispersion profile. As noted above, carboxyls with up-shifted pK_a values often have critical biological functions, e.g., in enzyme active sites, suggesting that these important cases should be particularly amenable to study by our method.

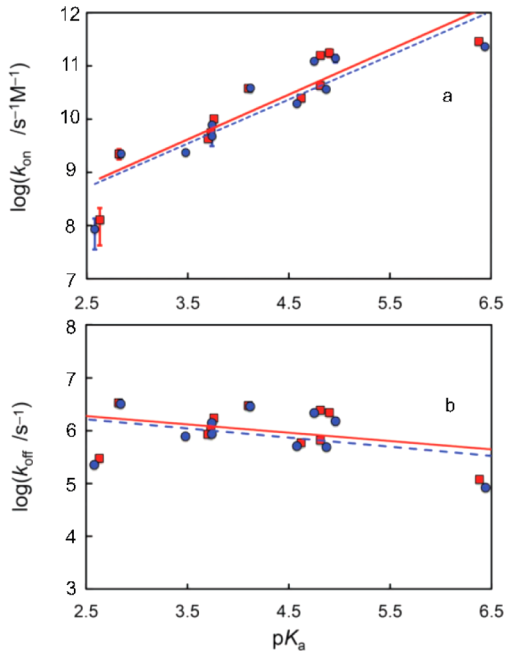

Figure 3. Free-energy relationships: logarithmic plots of rate constants vs equilibrium dissociation constants. (a) $\log_{10}(k_{on})$ and (b) $\log_{10}(k_{off})$ plotted vs pK_a. Blue circles and red squares indicate results obtained at 15 and 25 °C, respectively. Lines indicate least-squares linear fits to the data. Data are shown for all D and E residues in PGB-QDD, except for D36. Error bars (1 standard deviation) were determined by Monte Carlo simulations. For most residues the error bars are smaller than the symbol size. The correlation coefficients of the linear fits are r^2 = 0.82 (k_{on}, 15 °C), 0.80 (k_{on}, 25 °C), 0.14 (k_{off}, 15 °C), and 0.15 (k_{off}, 25 °C).

The relative error of the determined rate constant is reasonably low in all cases but varies significantly between residues, from <1% for for D37 to 17% for D22. The large variation in precision primarily reflects the amplitude of the relaxation dispersion (as a function of pH), i.e., the relative contribution from exchange (R_{ex}) to the observed transverse relaxation rates (R_2), see eq 7. In addition, a large difference between $R_{2,A}$ and $R_{2,HA}$ acts to mask the effect of modest R_{ex} contributions to the dispersion profile, as observed for D8 (Figure 2a), which impacts negatively on the achievable precision. At the maximum of the dispersion profile, R_{ex} depends on the chemical shift difference squared ($\Delta\omega^2$) and the proton-exchange rate (k_{ex}), see eq 5. D37 has a chemical shift difference between the protonated and unprotonated states of $\Delta\delta = \Delta\omega/(\gamma B_0)$ = 3.64 ppm and the lowest k_{off} of all residues, resulting in large relaxation dispersion amplitude (Figures 2b and S4) and high precision in the determined rate constants. By comparison, the low dispersion amplitude observed for E42 (Figure 2e), which has a chemical shift difference of $\Delta\delta$ = 4.10 ppm, directly indicates that it is undergoing fast proton exchange, where particularly k_{on} stands out as being among the higher rates measured in PGB1-QDD. Thus, the observation of a low dispersion amplitude for a residue with a sizable $\Delta\omega$ directly provides a qualitative indication that the proton-exchange rate is high. In fact, the quantitative measurement is accurate, despite the inherently low precision that results from the low dispersion amplitude. By contrast, k_{on} and k_{off} are poorly determined for those cases where the dispersion amplitude and $\Delta\omega$ both are small; D22 is a clear example of such a case.

To verify that proton exchange is indeed fast, we carried out carboxyl ^{13}C relaxation dispersion experiments, using either CPMG or $R_{1\rho}$ methods (see Figures S6 and S7 for representative examples). We specifically targeted D37, the residue with the lowest k_{off}, using $R_{1\rho}$ experiments. Experiments carried out at pH 7.48, where R_{ex} contributes significantly to R_2, result in a flat dispersion profile for D37 (Figure S6). Similar results were obtained for all residues, thus confirming the expectation that the proton-exchange rates are much higher than the achievable refocusing frequency, i.e., k_{ex} > 30,000 s^{-1} in the present case. Advancements in probe technology and radio frequency coil design should make it possible to measure relaxation dispersion as a function of refocusing frequency for carboxyl groups.[60]

The present method has the advantage that protonation kinetics is monitored directly on the ^{13}C of the acidic carboxyl group, which undergoes two-site exchange between the protonated and nonprotonated states, and whose chemical shift is strongly correlated with the relative populations of these states. Thus, the exchange broadening of the ^{13}C resonance can be directly interpreted in terms of proton exchange. This is in contrast to previous NMR methods to monitor proton exchange in carboxylic acids, which have focused on the relaxation broadening of water nuclei,[39−41] which requires a more complicated analysis due to the presence of a number of contributing exchange processes in addition to proton transfer to/from the carboxyl group. Our approach is also different in this respect from previous ^{15}N relaxation studies of pH-

DOI: 10.1021/ja513205s
J. Am. Chem. Soc. 2015, 137, 3093−3101

dependent exchange between alternative backbone conformations related to protonation equilibria of histidine residues.[61]

How do the measured rates compare with those reported previously for carboxylic acids? The present results are broadly in line with the rate constant for proton dissociation from acetic acid, k_{off} = 0.8 × 10^6 s^{-1},[11] and for deuteron exchange of carboxyl groups in basic pancreatic trypsin inhibitor and ubiquitin, k_{off} = 1.2 x 10^6 s^{-1}.[41] Proton transfer on-rates for carboxylic acids are expected to fall in the range from 10^9 to 10^{12} M^{-1} s^{-1},[11] in good agreement with the current results. Proton-transfer rates have been measured for internal acidic residues in membrane proteins using IR or absorbance spectroscopy, resulting in deprotonation rates that are considerably lower than those measured here. In bacteriorhodopsin, deprotonation reactions of internal aspartic residues coupled to proton pumping occur with rates on the order of 10^2 s^{-1}.[17] In cytochrome *c* oxidase the deprotonation rate of an internal glutamic residue has been estimated to 10^4 s^{-1}.[62] These examples are thus 1−3 orders of magnitude lower than the lowest rate measured for PGB1-QDD (viz. 0.120 × 10^6 s^{-1} for D37; see Table 1). An obvious difference between the two membrane proteins and PGB1-QDD is that the carboxyl groups are located in the protein interior in the former, but primarily solvent exposed in the latter. The variation in proton-exchange rates observed in PGB1-QDD and other systems is most likely the result of a combination of both electrostatic and nonelectrostatic factors, including hydrogen bonding and the extent of burial and flexibility of the titrating residue and its surroundings, which impact on water access to the exchanging site.

Hydrogen Bonding Explains Low and High Protonation Rates. To address the question whether specific interactions affect the protonation kinetics, we screened for hydrogen bonds involving the carboxyl groups, based on the PDB structure 1pgb.[50] We identified hydrogen bonds to the side-chain carboxyl group of residues D22, D46, D47, and E56. Interestingly, these four residues also have the lowest values of k_{on} and pK_a. By accepting a hydrogen bond from a neighboring residue, the charged carboxyl group is stabilized and clearly less likely to become protonated by the hydronium ions of the solvent.

In the wild-type protein, the side-chain amide of N37 hydrogen bonds to the backbone carbonyl of Y33 in a helix-capping fashion. It is likely that the protonated carboxyl group of D37 in PGB1-QDD serves the same function, thereby explaining, at least in part, its low k_{off}, high k_{on}, and highly upshifted pK_a value.[33] In this case, the hydrogen-bonded proton has a reduced tendency to be released to the solvent. This scenario, where the protonated carboxyl of D37 donates a hydrogen bond, is thus the counterpart of the hydrogen-bond-accepting side chains of D22, D46, D47, and E56. Together, these results provide a mechanistic view of how specific interactions affect the protonation kinetics.

Side-Chain Carbonyls Serve As Negative Controls. The relaxation rates of side-chain carbonyl ^{13}C nuclei in asparagine (N) and glutamine (Q) residues are not expected to show any significant variation with pH, since these nonionic moieties do not become protonated to any significant extent in the pH interval covered here. In keeping with this expectation, Q32 exhibits a flat profile of R_2 vs pH at both 15 and 25 °C (Figure 2c) and a very modest chemical shift difference ($\Delta\delta \approx$ 0.1 ppm) between the low and high pH limits. Similarly, Q2 and N35 both show only a minor increase in R_2 at lower pH ($\Delta R_2 \approx 0.5-1.0$ s^{-1}) and $\Delta\delta < 0.5$ ppm between the limiting pH values (Figures S2 and S4). The differences in chemical shift reflect the fact that also the uncharged side-chain carbonyl groups are affected by a local change in the electric field, and possibly also hydrogen bonding, between pH 1.9 and 8.5, as the surrounding charged groups titrate. The change in R_2 at low pH indicates that the fast (ps−ns) time-scale conformational dynamics of the side chain might depend on the local conformation and electrostatic potential, in agreement with the results obtained for the majority of acidic carboxyl groups in PGB1-QDD. However, overall the variation in R_2 and $\Delta\delta$ with pH is much reduced for N and Q residues, compared to that observed for D and E residues. Thus, we conclude that nonexchange mediated variation in R_2 does not exhibit the same response to changes in pH and is insignificant in comparison to the often sizable effects caused by proton-exchange dynamics.

Linear Free-Energy Relationships. Linear free-energy relationships in proton-transfer reactions have been investigated extensively by computational approaches.[14,63] We investigated whether linear free-energy relationships exist between the activation barrier and the free energy difference between the protonated and deprotonated states of the carboxyl side chains by plotting $\log_{10}(k)$ versus pK_a.[64,65] Assuming that pre-exponential factors (e.g., the transmission coefficient) in k_{off} and k_{on} do not vary appreciably among sites, linear free-energy relationships can be interpreted to derive information about the energy landscape of the proton-transfer reaction. Figure 3 shows plots of $\log_{10}(k_{on})$ and $\log_{10}(k_{off})$ versus pK_a. As observed, $\log_{10}(k_{on})$ shows an approximately linear relationship with pK_a, r^2 = 0.8 (Figure 3a), whereas the correlation with pK_a is not significant in the case of $\log_{10}(k_{off})$, r^2 = 0.15 (Figure 3b).

The fact that $\log_{10}(k_{on})$ correlates with pK_a, whereas $\log_{10}(k_{off})$ does not, indicates that the variations in k_{on} and K_a are governed mainly by the differences between side chains in the stabilization of their deprotonated states, as might be expected from electrostatic considerations. Conversely, the free energies of the transition state and of the protonated state apparently show less variation between side chains in PGB1-QDD. The data represented in Figure 3 thus provide insights into the energy landscape of proton transfer in proteins at the level of atomic resolution.

Limited Temperature Dependence of Proton-Exchange Kinetics. We measured complete R_2 vs pH profiles comprising 21 pH values at both 15 and 25 °C. Figures 2 and S4 show the effect of temperature on the R_2 profiles. The offset (at the pH extrema) between the two data sets arise from the difference in effective correlation times of rotational diffusion, which affect the intrinsic relaxation rates $R_{2,A}$ and $R_{2,HA}$, see eq 1, whereas the changes in amplitude and location of the dispersion maximum reflect the temperature dependence of k_{ex} and K_a, see eq 6. All carboxyl groups show values of k_{off} and k_{on} that are lower or equal (within errors) at 15 °C than at 25 °C (Table 1), as expected from theory. The good agreement between the two independent data sets provides additional validation of the results.

The difference in off-rates determined at the two temperatures is small, suggesting that the activation barrier of the deprotonation process is relatively low, in keeping with the high rates (>10^5 s^{-1} in all cases; cf. Table 1). The on-rate also shows a modest temperature dependence. Here, the higher viscosity at the lower temperature acts to reduce diffusion-limited on-rates, which contribute to the lower k_{on} values observed at 15 °C,

DOI: 10.1021/ja513205s
J. Am. Chem. Soc. 2015, 137, 3093−3101

compared to those at 25 °C. The relatively weak temperature dependence of k_{off} and k_{on} indicates that the activation barrier of proton transfer is generally low for carboxyls in PGB1-QDD.

Conformational Exchange Dynamics. D37 shows a bimodal variation in R_2 with pH (Figure S4). The high-pH dispersion profile corresponds to protonation kinetics, as described above, while the low-pH profile (with a maximum at pH ≈ 3.5) is caused by fast exchange between alternative conformational states, as described previously.[66] Other residues located nearby D37, namely N35 and D36, also show enhanced R_2 rates in the low-pH range (Figure S4), which appear to reflect the same conformational exchange process as D37. (The interpretation of D36 is compounded by the fact that its pK_a matches with the pH of maximum R_2, so that protonation exchange overlaps with conformational exchange in this case.) As noted above, the protonated carboxyl of D37 likely hydrogen bonds to the backbone of Y33, similar to the interaction observed between N37 and Y33 in the wild-type protein. Based on this assumption, we suggest that the observed conformational exchange involves transient breaking of the hydrogen bond between the D37 carboxyl and the backbone of Y33. The fact that the maximum of the R_2 dispersion for D37 in the low-pH regime matches with the pK_a value of D36 might indicate that protonation of the D36 carboxyl group destabilizes the helix and leads to fraying, as previously suggested,[66] and concomitant breaking of the D37−Y33 hydrogen bond.

The observed conformational exchange preceeds protein unfolding upon lowering of pH. Acid-induced unfolding of PGB1-QDD becomes noticeable in the ^{1}H−^{15}N heteronuclear single-quantum correlation spectroscopy spectrum only at pH < 2, where cross-peaks from the unfolded state start to appear. However, global unfolding is detectable by carboxyl/carbonyl ^{13}C CPMG relaxation dispersion experiments already at pH 2.2 (Figure S7). Global unfolding at low pH occurs with an exchange rate considerably lower than the conformational exchange attributed to helix fraying; the R_{ex} contribution from the former process is quenched by a CPMG refocusing frequency of 800 Hz, while the latter is not (cf. Figures S4 and S7). Hence, global unfolding does not affect the R_2 vs pH dispersion data.

CONCLUSIONS

We have presented a method to determine site-specific protonation kinetics for carboxylic side chains in proteins. The ^{13}C carboxyl nucleus normally experiences a large chemical shift difference of 3−4 ppm between the protonated and deprotonated states, which gives rise to a measurable pH-dependent exchange contribution to the transverse relaxation rate for off-rates below approximately 10^6 s^{-1}. The present results on PGB1-QDD indicate that the great majority of carboxylic proton-exchange rates falls in this regime, in agreement with previous measurements on simple carboxylic acids in aqueous solution and immobilized proteins.[11,40,41] We note that residues with up-shifted pK_a values are expected to have relatively low off-rates and significant relaxation dispersion profiles. Many functionally important carboxyl groups, such as those located in enzyme active sites, are expected to fall in this category, leading to the expectation that our method should be ideally suited to address biologically relevant cases.

A linear free-energy relationship is established between the activation energy of protonation and the free energy of acid dissociation, which indicates that the variation in k_{on} and K_a among residues can be explained primarily by the relative stabilization of the deprotonated state, while the free energies of the transition state and the protonated state show less variation. Extreme values of k_{on} and k_{off} in PGB1-QDD can be explained by hydrogen bonding, which stabilizes the deprotonated or protonated state, respectively. Together, these results provide unique information on the energy landscape and mechanisms of proton-transfer reactions.

An increasing number of NMR relaxation experiments have made it possible to study side-chain dynamics, including protonation kinetics of positively charged side chains. The method presented here adds to the range of biochemical phenomena that can be investigated by targeting the important class of proton-transfer reactions involving carboxyl groups of acidic side chains, which play critical roles in enzyme catalysis and proton pumping.

MATERIALS AND METHODS

Theory. The protonation equilibrium of carboxylic side chains is described by the reaction

$$\text{R-CO}_2\text{H} \rightleftharpoons \text{R-CO}_2^- + \text{H}^+$$

where H^+ collectively denotes hydronium ions and higher-order complexes.[67]

The measured transverse relaxation rate of the observed carboxyl ^{13}C spin is given by

$$R_2 = p_A R_{2,A} + p_{HA} R_{2,HA} + R_{ex} \quad (1)$$

where p_A and $p_{HA} = 1 - p_A$ denote the relative populations of the nonprotonated and protonated states of the carboxyl side chain, $R_{2,A}$ and $R_{2,HA}$ are the intrinsic transverse relaxation rates due to the dipole−dipole and chemical shift anisotropy relaxation mechanisms of the two states, and R_{ex} is the contribution to transverse relaxation from chemical exchange between states. Under conditions where the exchange kinetics is fast on the chemical shift time scale ($k_{ex} > \Delta\omega$), R_{ex} is given by[48]

$$R_{ex} = \frac{p_A p_{HA} \Delta\omega^2}{k_{ex}}[1 - 2\tan(k_{ex}\tau_{cp}/2)/(k_{ex}\tau_{cp})] \quad (2)$$

where $\Delta\omega$ is the frequency difference between these states, τ_{cp} is the delay between 180° refocusing pulses of the CPMG pulse train, and k_{ex} is the exchange rate, which is given by

$$k_{ex} = k_{on}[H^+] + k_{off} = k_{off}\left(\frac{[H^+]}{K_a} + 1\right) = \frac{k_{off}}{p_A} \quad (3)$$

where k_{on} and k_{off} are the on- and off-rates for proton exchange and K_a is the acid−base dissociation constant:

$$K_a = [H^+]\frac{p_A}{p_{HA}} \quad (4)$$

Under conditions where $k_{ex} \gg \Delta\omega$ and $k_{ex} \gg 1/\tau_{cp}$, R_{ex} is very well approximated (to the level of 0.1% relative error for $k_{ex} = 10^3\ \Delta\omega$ and $k_{ex} = 10^3/\tau_{cp}$, which are both fulfilled here; see Results and Discussion section) by the simplified expression

$$R_{ex} = \frac{p_A p_{HA} \Delta\omega^2}{k_{ex}} \quad (5)$$

Using eqs 3−5, R_{ex} can be expressed[68] as

$$R_{ex} = \frac{\Delta\omega^2}{k_{off}}\frac{x}{(1+x)^3} \quad (6)$$

where $x = [H^+]/K_a$. The function $R_{ex}(x)$ has a maximum at $x = 1/2$; that is, at pH = pK_a + $\log_{10}(2)$. Figure 4 illustrates the dependence of R_{ex} on pH for typical values of $\Delta\omega$ and k_{off}. Recasting eq 1 as a function of the parameter x, the observed relaxation rate is given by

DOI: 10.1021/ja513205s
J. Am. Chem. Soc. 2015, 137, 3093−3101

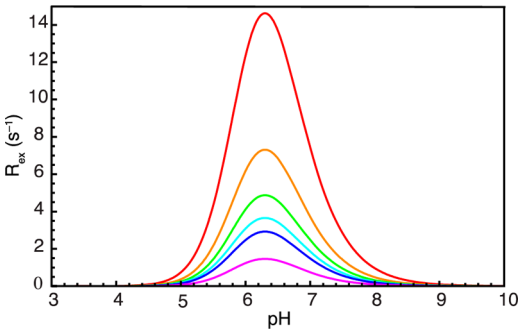

Figure 4. The pH-dependent exchange contributions to the transverse relaxation rate. R_{ex} is plotted using eq 6 as a function of pH for different values of k_{off}. k_{off} = {1, 2, 3, 4, 5, 10} × 10^5 s^{-1} colored {red, orange, green, cyan, blue, and magenta}, respectively. The chemical shift difference was set to $\Delta\delta = \Delta\omega/(\gamma B_0)$ = 4 ppm, which is typical for ^{13}C spins in E side-chain carboxyl groups. The pK_a was set to a representative value (pK_a = 6); the curves are identical for other values of pK_a but appear displaced along the horizontal axis, as described by eq 6. The maximum of R_{ex} occurs for pH = pK_a + $\log_{10}(2)$ ≈ pK_a + 0.3. The figure was produced using *Mathematica* (Wolfram Research, Inc.).

$$R_2 = R_{2,A}\frac{1}{1+x} + R_{2,HA}\frac{x}{1+x} + \frac{\Delta\omega^2}{k_{off}}\frac{x}{(1+x)^3} \quad (7)$$

Since both $\Delta\omega$ and pK_a can be determined separately with high accuracy and precision from the chemical shift versus pH titration curves,[32,33] it is evident from Figure 4 and eq 7 that measurement of R_2 as a function of pH should make it possible to determine k_{off} together with $R_{2,A}$ and $R_{2,HA}$, provided that k_{off} is sufficiently low and $\Delta\omega$ sufficiently large.

pK_a values were determined by monitoring the chemical shift as a function of pH:[69]

$$\delta_{obs} = \delta_A\frac{1}{1+x_H} + \delta_{HA}\frac{x_H}{1+x_H} \quad (8)$$

where δ_{obs} is the observed chemical shift, and δ_A and δ_{HA} are the chemical shifts of nonprotonated and protonated states, respectively, and x_H is given by

$$x_H = ([H^+]/K_a)^{n_H} \quad (9)$$

where n_H is the phenomenological Hill coefficient that represents the coupling among charged residues;[32,69] for n_H = 1, there is no coupling between the monitored residue and the surroundings. As described under Results and Discussion section, replacing x by x_H in eq 7 does not have any significant effect on the optimized parameters (k_{off}, $R_{2,A}$, and $R_{2,HA}$).

NMR Sample Preparation. The protein used in the present study is a variant of the PGB1, with three mutations introduced to avoid post-translational modifications: T2Q (to avoid N-terminal processing) and N8D and N37D (to avoid covalent rearrangement due to deamidation), denoted PGB1-QDD. The expression and purification protocols have been described previously.[53] All NMR samples contained 2.0 ± 0.2 mM ^{13}C/^{15}N-labeled PGB1-QDD dissolved in 90% dd-H_2O/10% D_2O (v/v). The pH was adjusted using 0−60 μL additions of 0.01 M HCl or NaOH. The pH was measured using a MP225 pH meter equipped with a combination electrode U402-M3-S7/200 (Mettler Toledo), calibrated with standard solutions of pH 4.01, 7.00, and 9.21. The pH was corrected by adding 0.04 units to the measured value in order to account for the 10% D_2O present in the sample. Separate samples were prepared for each pH value. In total, 21 samples were prepared with the following pH values: 1.91, 2.19, 2.44, 3.12, 3.40, 3.71, 4.08, 4.34, 4.63, 4.80, 4.93, 5.34, 5.51, 5.75, 6.16, 6.60, 6.69, 6.95, 7.48, 8.03, and 8.55. The pH readings are accurate to ±0.02 units.

NMR Spectroscopy. All experiments were performed on a Varian/Agilent VNMRS DirectDrive spectrometer operating at a magnetic field strength of 11.7 T. Resonance assignments of the D, E, N, and Q side-chains of PGB1-QDD have been reported.[53] Transverse relaxation rates of the ^{13}C carboxyl/carbonyl spins were measured at 21 different pH values ranging from 1.91 to 8.55, and 2 temperatures, 15.0 and 25.0 (±0.1) °C, using a H($C^{\beta/\gamma}$)CO-type experiment.[70] Intensity decays were sampled by 9 relaxation delays (T_{relax}), ranging from 0 to 80 ms in increments of 10 ms. The refocusing frequency of the CPMG train was fixed at ν_{CPMG} = 800 Hz. Each spectrum was recorded using 24−48 transients, 1200−1400 Hz spectral range sampled by 64−128 complex points in ω_1 (^{13}C), 8013 Hz sampled by 1024 complex points in ω_2 (^{1}H), and a recycle delay of 2.0 s, resulting in a net acquisition time for each pH data set of 22.5 h. For experiments acquired at low pH, the acquisition time was increased to 35−40 h to achieve improvement in both S/N and resolution.

^{13}C carboxyl/carbonyl CPMG and $R_{1\rho}$ relaxation dispersion experiments were performed at 3 pH values: 2.19, 4.08, and 7.48 at 25 °C, and at 7.48 at 15 °C, using the same H($C^{\beta/\gamma}$)CO pulse sequence as above,[70] or modifications thereof. CPMG data sets comprised 11 ν_{CPMG} values ranging from 40 to 920 Hz, with duplicates acquired for 3 ν_{CPMG} values to assess experimental errors. The relaxation period was 50 ms. $R_{1\rho}$ data sets comprised 9 spin-lock fields ranging from 900 to 5200 Hz, with the carrier placed at 176.32, 179.98, or 182.28 ppm to achieve near on-resonance spin-locks for different regions of the spectrum. Each spectrum was recorded using 32 (CPMG) or 24−32 ($R_{1\rho}$) transients, 1400 Hz spectral range sampled by 64 complex points in ω_1 (^{13}C), 8013 Hz sampled by 1024 complex points in ω_2 (^{1}H), with a recycle delay of 2.0 s, resulting in a net acquisition time for each pH data set of 36−45 h.

Data Analysis. All spectra were processed using NMRPipe.[71] A cosine-squared apodization function was used in the indirect dimension and either cosine or 30−50° shifted cosine functions in the direct dimension, as deemed optimal depending on the spectral resolution at each pH value. Peak intensities were extracted using CcpNmr Analysis.[72] R_2 was determined, at each pH and temperature, by fitting single-exponential functions to the peak intensity decays for each side-chain carboxyl/carbonyl group. Error estimates were obtained as the diagonal elements of the covariance matrix of the fitted parameters. The final sets of R_2 values covered 15−21 pH values, where the lower number was obtained in cases of peak overlap at certain pH values. In general, duplicate data points were obtained for each residue at a given pH, due to the presence of two $^1H^{\beta/\gamma}$−^{13}CO cross-peaks in the spectrum, except in those cases where the two $^1H^{\beta/\gamma}$ chemical shifts are degenerate.

The parameters of eq 8, i.e., δ_A, δ_{HA}, pK_a, and n_H, were fitted to the chemical shift titration curves (δ_{obs} vs pH), using the Levenberg−Marquardt optimization routine[73,74] implemented in Matlab (R2014a-b; The MathWorks, Inc.). In the same manner, the parameters of eq 7 were fitted to the experimental data sets, R_2 vs pH, while keeping $\Delta\omega$ fixed at the value obtained from the chemical shift titrations. Nested models were applied to test whether a given relaxation data set required fitting of both $R_{2,A}$ and $R_{2,HA}$ (i.e., $R_{2,A} \neq R_{2,HA}$), or could be fit with $R_{2,A} = R_{2,HA}$; these tests employed the F-statistic at the level of $p < 0.01$.[75] Similarly, the inclusion of K_a as a free parameter of the fit was tested for all residues, at the level of $p < 0.01$, in order to monitor whether the results deviated from those obtained when using a fixed value of K_a, taken from the chemical shift titrations. Error estimates on the fitted parameters were obtained as the standard deviation from 300 Monte Carlo simulations[74] of the fit to eqs 7 or 8.

■ ASSOCIATED CONTENT

Supporting Information

$^1H^{\gamma/\delta}$−^{13}CO correlation spectra of PGB1-QDD acquired at 25 °C and 21 different pH values; carboxyl/carbonyl ^{13}C chemical shifts vs pH titration curves for all D, E, N, and Q residues in PGB1-QDD; comparison of pK_a values determined for carboxyl groups in PGB-QDD by Lindman et al.[53] and us; R_2 vs pH relaxation dispersion profiles for all D, E, N, and Q residues in PGB1-QDD; correlation plots of pK_a values determined from

DOI: 10.1021/ja513205s
J. Am. Chem. Soc. 2015, 137, 3093−3101

chemical shift titrations and R_2 vs pH data; carboxyl ^{13}C $R_{1\rho}$ relaxation dispersion profile for D37; carboxyl ^{13}C CPMG relaxation dispersion profiles for D8 and N35; tables summarizing fitted parameters (pK_a, $\Delta\delta$, n_H) and *F*-statistics of model selection in fitting eq 8; table summarizing model selection in fitting eq 7. This material is available free of charge via the Internet at http://pubs.acs.org.

AUTHOR INFORMATION

Corresponding Author

*mikael.akke@bpc.lu.se

Notes

The authors declare no competing financial interest.

ACKNOWLEDGMENTS

We thank Kristofer Modig for helpful discussions on model fitting and error analysis. This work was supported by the Swedish Research Council (621-2010-4912), the Göran Gustafsson Foundation for Research in Natural Sciences and Medicine, and the Knut and Alice Wallenberg Foundation.

REFERENCES

(1) Perutz, M. F. *Science* **1978**, *201*, 1187.
(2) Warshel, A. *Biochemistry* **1981**, *20*, 3167.
(3) Sharp, K. A.; Honig, B. *Annu. Rev. Biophys. Biophys. Chem.* **1990**, *19*, 301.
(4) Schaefer, M.; Van Vlijmen, H. W. T.; Karplus, M. *Adv. Protein Chem.* **1998**, *51*, 1.
(5) Warshel, A.; Sharma, P. K.; Kato, M.; Parson, W. W. *Biochim. Biophys. Acta, Proteins Proteomics* **2006**, *1764*, 1647.
(6) Lund, M.; Jonsson, B. *Q. Rev. Biophys.* **2013**, *46*, 265.
(7) Forsyth, W. R.; Antosiewicz, J. M.; Robertson, A. D. *Proteins: Struct., Funct., Bioinf.* **2002**, *48*, 388.
(8) Castaneda, C. A.; Fitch, C. A.; Majumdar, A.; Khangulov, V.; Schlessman, J. L.; Garcia-Moreno, B. E. *Proteins: Struct., Funct., Bioinf.* **2009**, *77*, 570.
(9) Simonson, T.; Carlsson, J.; Case, D. A. *J. Am. Chem. Soc.* **2004**, *126*, 4167.
(10) Nielsen, J. E.; Mccammon, J. A. *Protein Sci.* **2003**, *12*, 1894.
(11) Eigen, M. *Angew. Chem., Int. Ed.* **1964**, *3*, 1.
(12) Fersht, A. *Structure and mechanism in protein science. A guide to enzyme catalysis and protein folding*; 1st ed.; W.H. Freeman & Co.: New York, 1999.
(13) Holliday, G. L.; Almonacid, D. E.; Mitchell, J. B. O.; Thornton, J. M. *J. Mol. Biol.* **2007**, *372*, 1261.
(14) Warshel, A.; Hwang, J. K.; Aqvist, J. *Faraday Discuss.* **1992**, *93*, 225.
(15) Ferguson, S. J. *Curr. Biol.* **2000**, *10*, R627.
(16) Gerwert, K.; Hess, B.; Soppa, J.; Oesterhelt, D. *Proc. Natl. Acad. Sci. U.S.A.* **1989**, *86*, 4943.
(17) Gerwert, K.; Souvignier, G.; Hess, B. *Proc. Natl. Acad. Sci. U.S.A.* **1990**, *87*, 9774.
(18) Abrahams, J. P.; Leslie, A. G. W.; Lutter, R.; Walker, J. E. *Nature* **1994**, *370*, 621.
(19) Iwata, S.; Ostermeier, C.; Ludwig, B.; Michel, H. *Nature* **1995**, *376*, 660.
(20) Tsukihara, T.; Aoyama, H.; Yamashita, E.; Tomizaki, T.; Yamaguchi, H.; ShinzawaItoh, K.; Nakashima, R.; Yaono, R.; Yoshikawa, S. *Science* **1996**, *272*, 1136.
(21) Kaila, V. R. I.; Wikstrom, M.; Hummer, G. *Proc. Natl. Acad. Sci. U.S.A.* **2014**, *111*, 6988.
(22) Kato, M.; Pisliakov, A. V.; Warshel, A. *Proteins: Struct., Funct., Bioinf.* **2006**, *64*, 829.
(23) Johansson, A. L.; Chakrabarty, S.; Berthold, C. L.; Hogbom, M.; Warshel, A.; Brzezinski, P. *Biochim. Biophys. Acta, Bioenerg.* **2011**, *1807*, 1083.
(24) Holliday, G. L.; Mitchell, J. B. O.; Thornton, J. M. *J. Mol. Biol.* **2009**, *390*, 560.
(25) Aqvist, J.; Warshel, A. *Biochemistry* **1989**, *28*, 4680.
(26) Sigala, P. A.; Fafarman, A. T.; Schwans, J. P.; Fried, S. D.; Fenn, T. D.; Caaveiro, J. M. M.; Pybus, B.; Ringe, D.; Petsko, G. A.; Boxer, S. G.; Herschlag, D. *Proc. Natl. Acad. Sci. U.S.A.* **2013**, *110*, E2552.
(27) Fried, S. D.; Boxer, S. G. *Proc. Natl. Acad. Sci. U.S.A.* **2013**, *110*, 12271.
(28) Gorfe, A. A.; Ferrara, P.; Caflisch, A.; Marti, D. N.; Bosshard, H. R.; Jelesarov, I. *Proteins: Struct., Funct., Genet.* **2002**, *46*, 41.
(29) Beroza, P.; Fredkin, D. R.; Okamura, M. Y.; Feher, G. *Proc. Natl. Acad. Sci. U.S.A.* **1991**, *88*, 5804.
(30) Beroza, P.; Case, D. A. *Methods Enzymol.* **1998**, *295*, 170.
(31) Marx, D. *ChemPhysChem* **2006**, *7*, 1848.
(32) Markley, J. L. *Acc. Chem. Res.* **1975**, *8*, 70.
(33) Lindman, S.; Linse, S.; Mulder, F. A. A.; Andre, I. *Biophys. J.* **2007**, *92*, 257.
(34) Kesvatera, T.; Jönsson, B.; Thulin, E.; Linse, S. *J. Mol. Biol.* **1996**, *259*, 828.
(35) Kesvatera, T.; Jönsson, B.; Thulin, E.; Linse, S. *Proteins: Struct., Funct., Genet.* **1999**, *37*, 106.
(36) Kesvatera, T.; Jönsson, B.; Thulin, E.; Linse, S. *Proteins: Struct., Funct., Genet.* **2001**, *45*, 129.
(37) Haupts, U.; Maiti, S.; Schwille, P.; Webb, W. W. *Proc. Natl. Acad. Sci. U.S.A.* **1998**, *95*, 13573.
(38) Widengren, J.; Terry, B.; Rigler, R. *Chem. Phys.* **1999**, *249*, 259.
(39) Luz, Z.; Meiboom, S. *J. Am. Chem. Soc.* **1963**, *85*, 3923.
(40) Lankhorst, D.; Schriever, J.; Leyte, J. C. *Chem. Phys.* **1983**, *77*, 319.
(41) Persson, E.; Halle, B. *J. Am. Chem. Soc.* **2008**, *130*, 1774.
(42) Liepinsh, E.; Otting, G. *Magnet Reson Med.* **1996**, *35*, 30.
(43) Kateb, F.; Pelupessy, P.; Bodenhausen, G. *J. Magn. Reson.* **2007**, *184*, 108.
(44) Segawa, T.; Kateb, F.; Duma, L.; Bodenhausen, G.; Pelupessy, P. *ChemBioChem* **2008**, *9*, 537.
(45) Sehgal, A. A.; Duma, L.; Bodenhausen, G.; Pelupessy, P. *Chem.—Eur. J.* **2014**, *20*, 6332.
(46) Hansen, P. E.; Feeney, J.; Roberts, G. C. K. *J. Magn. Reson.* **1975**, *17*, 249.
(47) Solomon, I. *C. R. Hebd. Seances Acad. Sci.* **1959**, *248*, 92.
(48) Luz, Z.; Meiboom, S. *J. Chem. Phys.* **1963**, *39*, 366.
(49) Palmer, A. G.; Grey, M. J.; Wang, C. Y. *Methods Enzymol.* **2005**, *394*, 430.
(50) Gallagher, T.; Alexander, P.; Bryan, P.; Gilliland, G. L. *Biochemistry* **1994**, *33*, 4721.
(51) Pettersen, E. F.; Goddard, T. D.; Huang, C. C.; Couch, G. S.; Greenblatt, D. M.; Meng, E. C.; Ferrin, T. E. *J. Comput. Chem.* **2004**, *25*, 1605.
(52) Khare, D.; Alexander, P.; Antosiewicz, J.; Bryan, P.; Gilson, M.; Orban, J. *Biochemistry* **1997**, *36*, 3580.
(53) Lindman, S.; Linse, S.; Mulder, F. A. A.; Andre, I. *Biochemistry* **2006**, *45*, 13993.
(54) Lindman, S.; Xue, W. F.; Szczepankiewicz, O.; Bauer, M. C.; Nilsson, H.; Linse, S. *Biophys. J.* **2006**, *90*, 2911.
(55) Lindman, S.; Bauer, M. C.; Lund, M.; Diehl, C.; Mulder, F. A. A.; Akke, M.; Linse, S. *Biophys. J.* **2010**, *99*, 3365.
(56) Tomlinson, J. H.; Green, V. L.; Baker, P. J.; Williamson, M. P. *Proteins: Struct., Funct., Bioinf.* **2010**, *78*, 3000.
(57) Tomlinson, J. H.; Ullah, S.; Hansen, P. E.; Williamson, M. P. *J. Am. Chem. Soc.* **2009**, *131*, 4674.
(58) Onufriev, A.; Case, D. A.; Ullmann, G. M. *Biochemistry* **2001**, *40*, 3413.
(59) Nielsen, J. E. *Methods Enzymol.* **2009**, *454*, 233.
(60) Smith, C. A.; Ban, D.; Pratihar, S.; Giller, K.; Schwiegk, C.; de Groot, B. L.; Becker, S.; Griesinger, C.; Lee, D. *Angew. Chem., Int. Ed. Engl.* **2014**, In press.
(61) Hass, M. A. S.; Thuesen, M. H.; Christensen, H. E. M.; Led, J. J. *J. Am. Chem. Soc.* **2004**, *126*, 753.

DOI: 10.1021/ja513205s
J. Am. Chem. Soc. 2015, 137, 3093−3101

(62) Johansson, A. L.; Carlsson, J.; Hogbom, M.; Hosler, J. P.; Gennis, R. B.; Brzezinski, P. *Biochemistry* **2013**, *52*, 827.
(63) Schutz, C. N.; Warshel, A. *J. Phys. Chem. B* **2004**, *108*, 2066.
(64) Leffler, J. E. *Science* **1953**, *117*, 340.
(65) Wells, T. N. C.; Fersht, A. R. *Biochemistry* **1989**, *28*, 9201.
(66) Tomlinson, J. H.; Craven, C. J.; Williamson, M. P.; Pandya, M. J. *Proteins: Struct., Funct., Bioinf.* **2010**, *78*, 1652.
(67) Marx, D.; Tuckerman, M. E.; Hutter, J.; Parrinello, M. *Nature* **1999**, *397*, 601.
(68) Paquin, R.; Ferrage, F.; Mulder, F. A. A.; Akke, M.; Bodenhausen, G. *J. Am. Chem. Soc.* **2008**, *130*, 15805.
(69) Markley, J. L. *Biochemistry* **1973**, *12*, 2245.
(70) Hansen, A. L.; Kay, L. E. *J. Biomol. NMR* **2011**, *50*, 347.
(71) Delaglio, F.; Grzesiek, S.; Vuister, G. W.; Zhu, G.; Pfeifer, J.; Bax, A. *J. Biomol. NMR* **1995**, *6*, 277.
(72) Vranken, W. F.; Boucher, W.; Stevens, T. J.; Fogh, R. H.; Pajon, A.; Llinas, P.; Ulrich, E. L.; Markley, J. L.; Ionides, J.; Laue, E. D. *Proteins: Struct., Funct., Bioinf.* **2005**, *59*, 687.
(73) Marquardt, D. *SIAM J. Appl. Math.* **1963**, *11*, 431.
(74) Press, W. H.; Flannery, B. P.; Teukolsky, S. A.; Vetterling, W. T. *Numerical Recipes. The Art of Scientific Computing*; Cambridge University Press: Cambridge, 1986.
(75) Bevington, P. R.; Robinson, D. K. *Data reduction and error analysis for the physical sciences*; WCB/McGraw-Hill: New York, 1992.

DOI: 10.1021/ja513205s
J. Am. Chem. Soc. 2015, 137, 3093−3101